Electronic Supplementary Material (ESI) for Inorganic Chemistry Frontiers.

Supporting information

Cu-Ni Alloy Decorating N-Doped Carbon Nanosheets toward High-performance Electrocatalysis of Mildly Acidic CO_2 Reduction

Weifan Pan[a,b], Peng Wang[a], Linfeng Fan[a], Kai Chen[a], Luocai Yi[a], Junheng Huang[a], Pingwei Cai[a], Xi Liu[a], Qingsong Chen[a], Genxiang Wang[a*], Zhenhai Wen[a*]

[a] *CAS Key Laboratory of Design and Assembly of Functional Nanostructures, and Fujian Provincial Key Laboratory of Materials and Techniques toward Hydrogen Energy, Fujian Institute of Research on the Structure of Matter, Chinese Academy of Sciences, Fuzhou, Fujian, 350002, China*

[b] *University of Chinese Academy of Sciences, Bejing 100049, China*

1. Materials

Raw materials involved in this work include phenol (AR, 99%), formaldehyde (AR, 37 wt%), sodium hydroxide (AR 96%), pluronic F-127, Zinc nitrate hexahydrate (AR, 98%), copper (II) nitrate hexahydrate (AR, 99%), nickel (II) nitrate hexahydrate (AR, 98%), 2-methylimidazole, hydrochloric acid, ethyl alcohol, isopropanol. The Nafion (5%) was purchased from Aladdin, and carbon paper was obtained from Hesen (HCP135), respectively. All reagents were used as received.

2. Methods

Electrochemical measurements were performed on a CHI 760E electrochemical workstation (ShangHai, China) with a three-electrode system in typical H-Cell (GaossUnion, TianJin) / Flow cell (self-assembly) separated by Nafion*117 (Dupond) membrane between cathode and anode. Gas phase products were analyzed by Gas Chromatography (SHIMADZU GC2014). Liquid product was detected by nuclear magnetic resonance spectrometer (^{1}HNMR) on ECZ600R. Microstructure images were taken using field emission scanning electron microscope (SEM, SU-8010). High-resolution TEM images as well as element mapping were obtained using tranmission electron microscope (TEM, Tecnai F20). The raman spectrums were performed on a Renishaw InVia Raman Microscope (532). X-ray diffraction spectra were taken by a Rigaku Miniflex 600 powder diffractometer. X-ray photoelectron spectra were carried out using ESCALAB 250Xi. The metal content was measured by Inductive Coupled Plasma Emission Spectrometer (Ultima 2).

2.1 Preparation of Resol-F127 solution.

The Resol-F127 solution was prepared undergoing the following steps: 0.6 g phenol, formaldehyde solution (2.1 mL, 37 wt% in H_2O), and an aqueous NaOH solution (15 mL, 0.1 M) were mixed and stirred at 70 ℃ for 30 min in a three-necked flask to obtain low-molecular-weight phenolic resols. Then, 65 mL aqueous solution containing 0.96 g F-127 was added and keep stirring under 340 rpm at 65 ℃ for further 15 h.

2.2 Preparation of CuNi-ZIF-8 suspension.

Typically, CuNi-ZIF-8 suspension liquid were synthesized using a one-step method in aqueous solution at room temperature. First, 0.8925 g $Zn(NO_3)_2{\cdot}6H_2O$, 0.0363 g $Cu(NO_3)_2{\cdot}3H_2O$ and 0.0436 g $Ni(NO_3)_2{\cdot}6H_2O$ were dissolved in 25 mL DI water via vigorously stirring to get a homogenous solution A. 1.2 g 2-methylimidazole was dissolved in 25 mL DI water to prepare solution B. Subsequently, poured solution A to solution B, and kept the reaction under ultrasonic processing for 1 h.

2.3 Preparation of Resol-F127 @ CuNi-ZIF-8 Composite.

24mL CuNi-ZIF-8 suspension, 8 mL Resol-F127 solution were thoroughly mixed by stirring for 30 min. Then the mixed suspension was transferred to a Teflon-lined autoclave for reaction at 150 ℃ for 20 h at a heating rate of 4 ℃ min^{-1} to reaction temperature. Following completion of the reaction, the autoclave was allowed to cool down to room temperature. After centrifugation and washed by water, the product was dried in a lyophilizer for 24 h to obtain Resol-F127 @ CuNi-ZIF-8 composite.

2.4 Synthesis of CuNi-N-CNS

A freshly prepared resol-F127 @ CuNi-ZIF-8 composite was transferred to a tube furnace and carbonized under a Ar atmosphere at 350 ℃ for 1 h, then at 900 ℃ for 2 h with a heating rate of 3 ℃ min^{-1}. After cooling to room temperature, the powder obtained was immersed in 2 M hydrochloric acid for 2 h to remove unstable metal impurities. The CuNi-N-CNS was then obtained after centrifugation, washing and drying.

2.5 Synthesis of contrast samples

The controlled samples, *i. e.* Ni-N-CNS, Cu-N-CNS and N-CNS, were prepared by the similar method with that of CuNi-N-CNS apart from without addition of Cu salt, Ni salt, and metal salts, respectively.

3. CO_2RR performance evaluation

3.1 H-type cell

Electrolysis was performed in a gas-tight H-type electrolyzer separating by a cation exchange membrane (Nafion 117). The Ag|AgCl electrode, platinum mesh (1*1 cm^2) and carbon paper (1*1 cm^2) acted as the reference electrode, counter electrode and work electrode, respectively. The work electrode was fabricated as the following processes: 100 μL of the catalyst ink was drop-casted on carbon paper electrode to achieve an approximately 1mg cm^{-2} loading amount and then dried under an infrared light. And 0.5 M $KHCO_3$ aqueous solution was used as the electrolyte, and the electrolyte was bubbled with CO_2 at least 20 min with a flow rate of 20 mL min^{-1} before electrolysis, the pH of the CO_2 saturated 0.5 M $KHCO_3$ was about 7.25. Then 1mL of gas was injected into gas chromatography from the outlet to analyze the composition of gas phase products. The detectors are calibrated by two different concentrations (H_2: 99.3 ppm and 10000 ppm; CO: 99.3 ppm and 10000 ppm) of standard gases.

3.2 Flow cell

Self-assembly flow cell was used to achieve great CO_2RR performance at high current densities. The device generally included a cathode chamber, an anode chamber and a proton exchange membrane (see Fig. 4a and supplementary Fig. S19). A commercial RuIrTi mesh is used as anode and an Ag|AgCl is acted as the reference. 3 M KCl and 1 M KOH are used as the cathode and anode electrolyte, respectively. The cathode chamber and anode chamber is separated by a piece of Nafion 117 membrane. Electrolytes are cycled at 100 mL min^{-1} and the CO_2 gas is supplied at rate of 20 mL min^{-1}. The pH of CO_2 saturated 3 M KCl presents a mildly acid environment with pH 4.25.

4. Electrochemical measurement in three-electrode system

All the potentials were quoted with respect to reversible hydrogen electrode (RHE) through RHE calibration according to the formula:

E (*vs.* RHE) = E (*vs.* Ag|AgCl) + E□ (Ag|AgCl) + 0.059 × pH

E (*vs.* RHE) = E (*vs.* Ag|AgCl + 0.197 V + 0.059 × pH **(Eq. 1)**

The faradaic efficiency of gas product was calculated based on the following equation **(Eq. 2)**:

$$FE = \frac{nzF}{Q} = \frac{PV_x}{RT} \times \frac{zF}{\int i\,dt} \quad \textbf{(Eq. 2)}$$

Where z is the number of electrons transferred per mole of gas products, n is the amount of substance of product, F is Faradaic constant 96485 C/mol, Q and $\int i\,dt$ are total passed charge within time t. And t is the time that needs to fill the sample injector at a constant CO_2 gas flow rate, V_x is the volume fraction of the obtained gaseous product i with time t (s), P is atmospheric pressure ($1.01*10^5$ Pa), T is the temperature, R is the gas constant (8.314 J mol^{-1} K^{-1}).

The partial current density of j_{CO} was calculated as following equation **(Eq. 3)**

$$j_{CO} = FE(CO) \times \frac{\int idt}{t} \quad \textbf{(Eq. 3)}$$

The turn over frequency (TOF, h^{-1}) was calculated as following equation **(Eq. 4)**

$$TOF = \frac{jco * A/zF}{m_{cat}{}^{w}/M} \times 3600 \quad (Eq.\ 4)$$

A: the surface area of the electrode (1 cm^{-2})

z: the number of electron transferred for CO production

j_{CO}: the partial current density (mA cm^{-2})

F: Faradaic constant 96485 C/mol

m_{cat}: the mass loading on the work electrode (mg)

W: Ni or Cu weight loading in the catalyst based on the ICP results.

The liquid products from were detected by H1NMR. 500 μL electrolyte after electrolysis was mixed with 100 μL D_2O containing 0.3 μL DMSO.

Table S1. ICP-OES results of CuNi-N-CNS.

Elements	Cu	Ni
Wt%	2.60%	2.39%

Table S2. The E-CO_2RR performance of recent reported catalysts.

Catalysts	Electrolyte	Electrolyzer	Long-term test	Potential	Current density	FE(CO)	Reference
Ni/Cu-N-C	0.5 M $KHCO_3$	H-Cell	60 h	-0.79 V *vs.* RHE	-30 mA cm^{-2}	99.2%	[1]
Ni/Fe-N-C	0.5 M $KHCO_3$	H-Cell	30 h	-0.7 V *vs.* RHE	-7.4 mA cm^{-2}	98.0%	[2]
NiSA/PCFM	0.5 M $KHCO_3$	H-Cell	15 h	-1.0 V *vs.* RHE	-28 mA cm^{-2}	87.0%	[3]
Ni-N-CNS/CNT	1 M KOH	Flow Cell	26 h	-0.73 V to -1.1 V	-100 mA cm^{-2} (constant current)	98.3%	[4]
Ni-N_4/C-NH_2	0.5 M $KHCO_3$	H-Cell	10 h	-0.8 V *vs.* RHE	-50 mA cm^{-2}	90.0%	[5]
Ni-N-MEGO	0.5 M $KHCO_3$	H-Cell	21 h	-0.55 V *vs.* RHE	-13.7 mA cm^{-2}	89.0%	[6]
Ni-NG	0.5 M $KHCO_3$	H-Cell	20 h	-0.64 V *vs.* RHE	-11 mA cm^{-2}	85.0%	[7]
Ni-NG	0.1 M $KHCO_3$	Flow Cell	8 h	2.78 V (cell voltage)	50 mA cm^{-2}	90.0%	[7]
Ni/HMCS-3-800	0.5 M $KHCO_3$	H-Cell	10 h	-0.9 V *vs.* RHE	6 mA cm^{-2}	90.0%	[8]
CuNi-N-CNS	0.5 M $KHCO_3$	H-Cell	50 h	-0.74 V *vs.* RHE	15 mA cm^{-2} to 10 mA cm^{-2}	~95.0%	This work
CuNi-N-CNS	3 M KCl	Flow cell	20 h	-0.82 V *vs.* RHE	200 mA cm^{-2} to 100 mA cm^{-2}	99% to 90%	This work

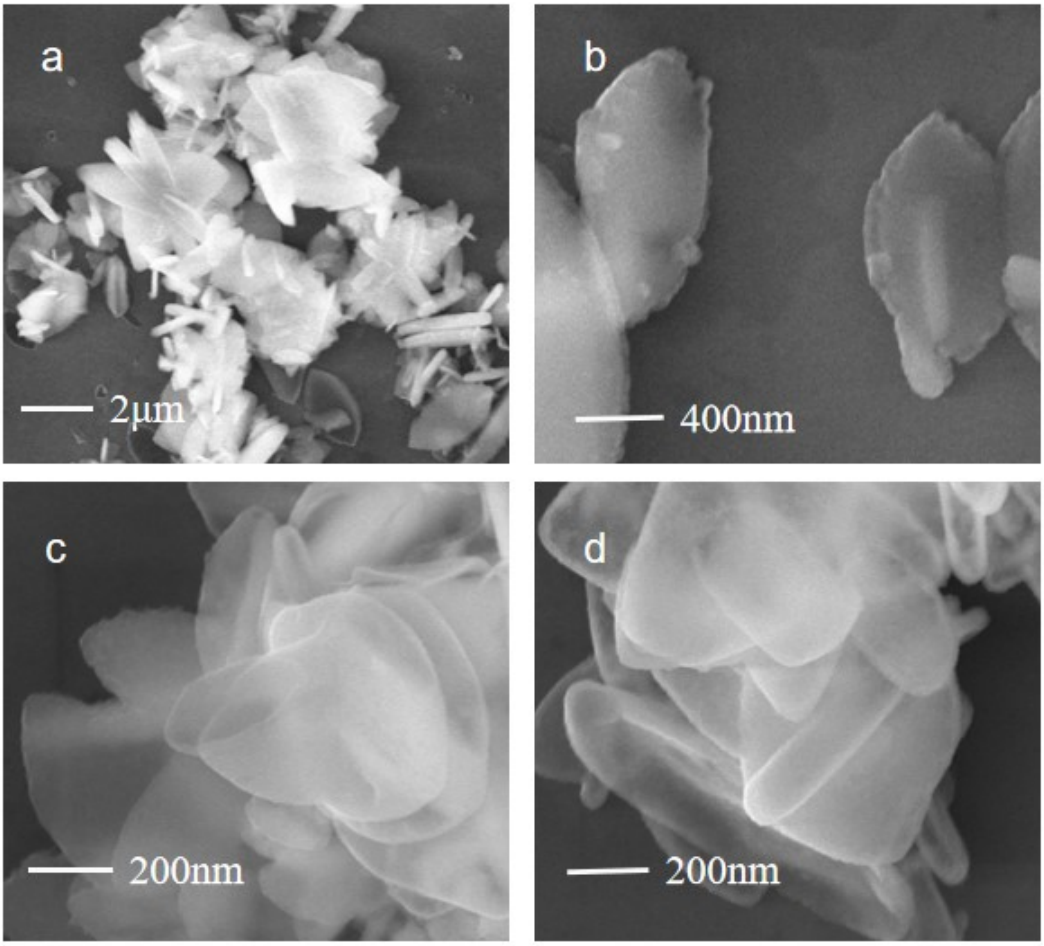

Figure S1. SEM (a-b) images for the first-step precursor (CuNi-ZIF-8) of CuNi-N-CNS. SEM (c-d) images for the second-step precursor (CuNi-ZIF-8 + Resol-F127-120℃) after hydrothermal reaction

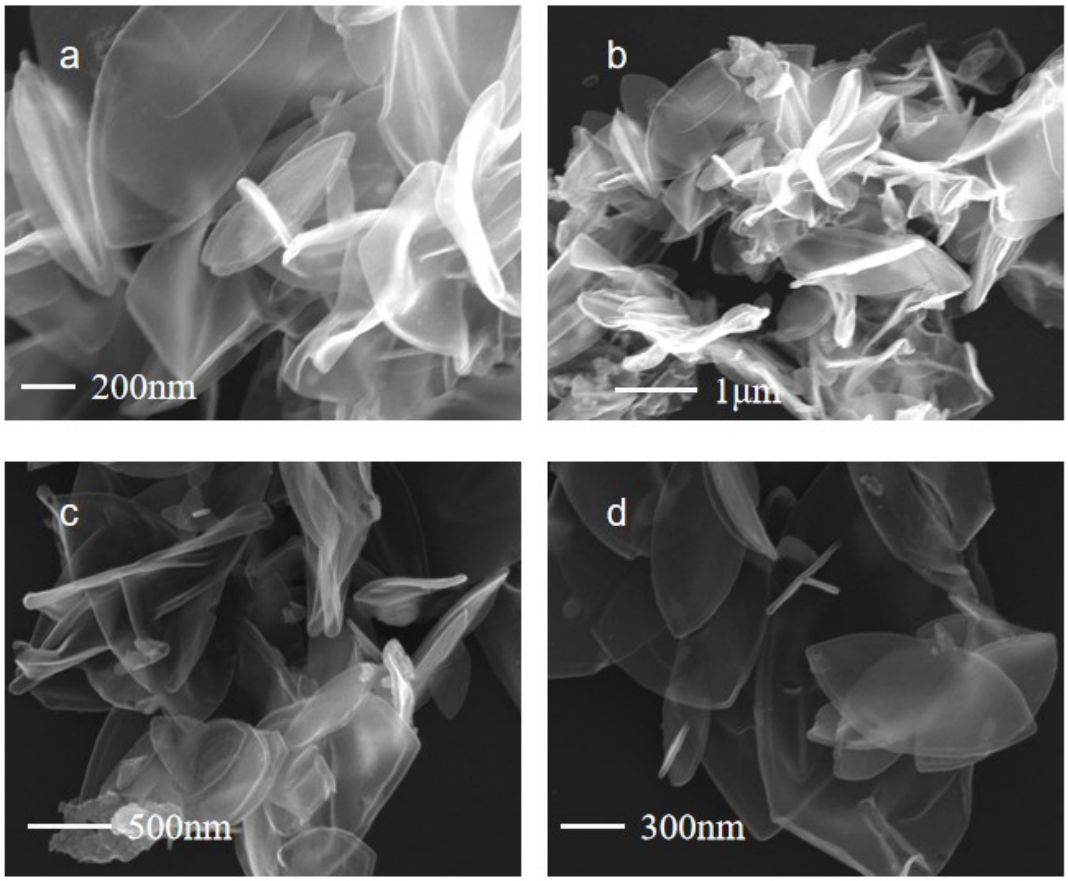

Figure S2. SEM patterns of (a) CuNi-N-CNS, (b) Ni-N-CNS, (c) Cu-N-CNS, (d) N-CNS.

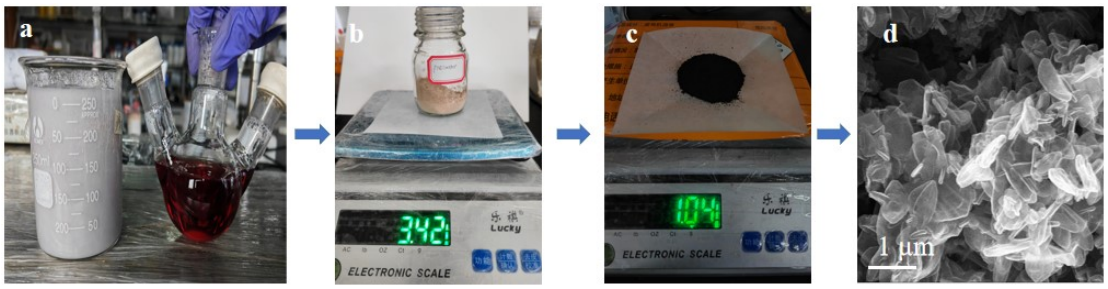

Figure S3. Gram-scale production of CuNi-N-CNS.

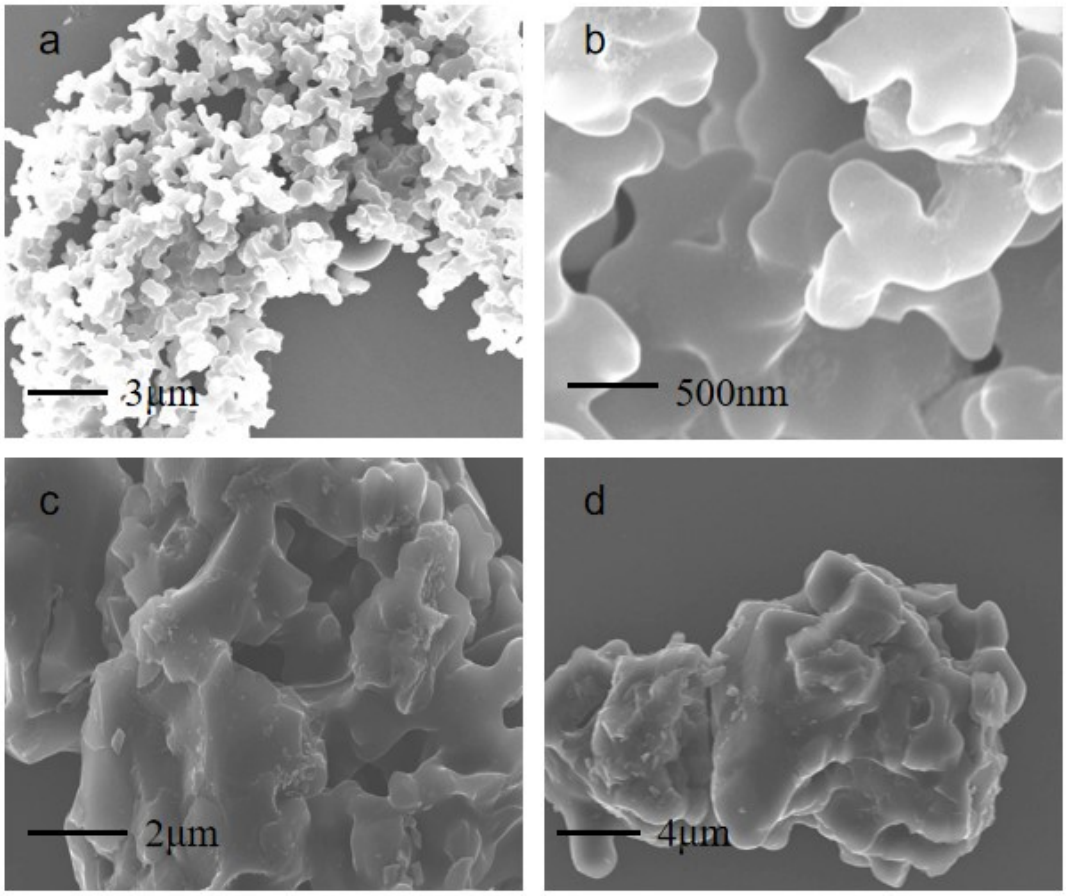

Figure S4. (a-b) SEM images of Resol-F127 after 900℃ pyrolysis. (c-d) SEM images of samples without Resol-F127 after pyrolysis, which show an irregular collapsed bulk structure.

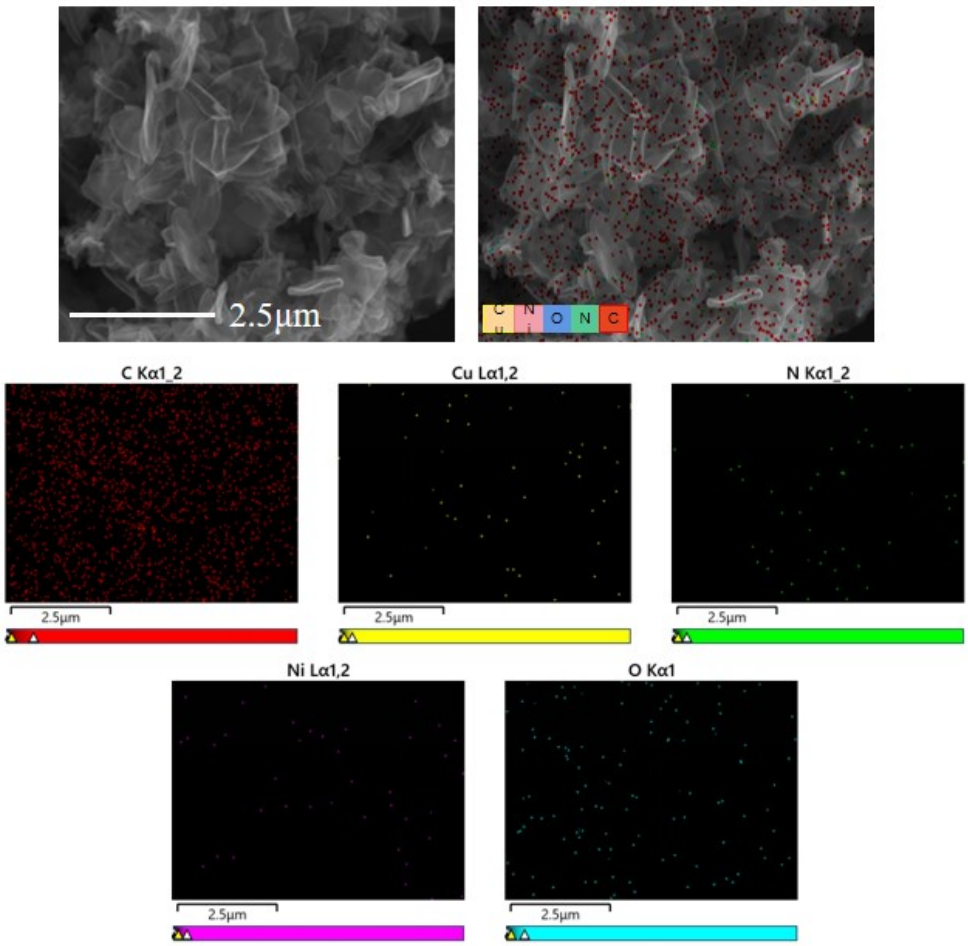

Figure S5. EDS of CuNi-N-CNS.

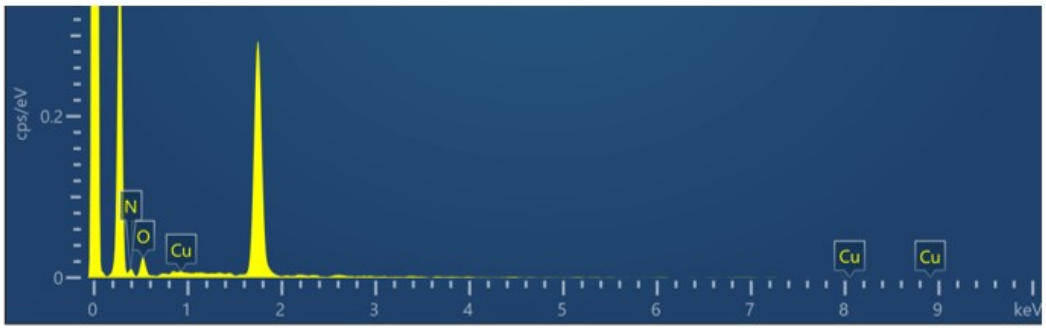

Element	Spectra type	Weight percentage	Wt % Sigma	Atomic percentage
C	K series spectra	73.68	3.98	79.26
N	K series spectra	12.79	3.92	11.80
O	K series spectra	10.18	1.71	8.22
Ni	L series spectra	2.09	1.74	0.46
Cu	L series spectra	1.27	1.35	0.26
Total content		100.00		100.00

XPS of CuNi-N-CNS				
Name	Peak BE	FWHM eV	Area(P) CPS.eV	Atomic %
C1s	284.97	3.1	1285440.28	84.48
O1s	532.22	3.76	324212.07	8.39
N1s	399.33	4.35	150938.69	6.25
Ni2p	854.95	3.52	109919.86	0.73
Cu2p1	951.97	1.75	3956.38	0.05
Cu2p3	933.24	2.10	14067.86	0.08
Cu LM2	567.00	0.54	3184.08	0.02

Figure S6. Comparison of element content results between EDS and XPS of CuNi-N-CNS.

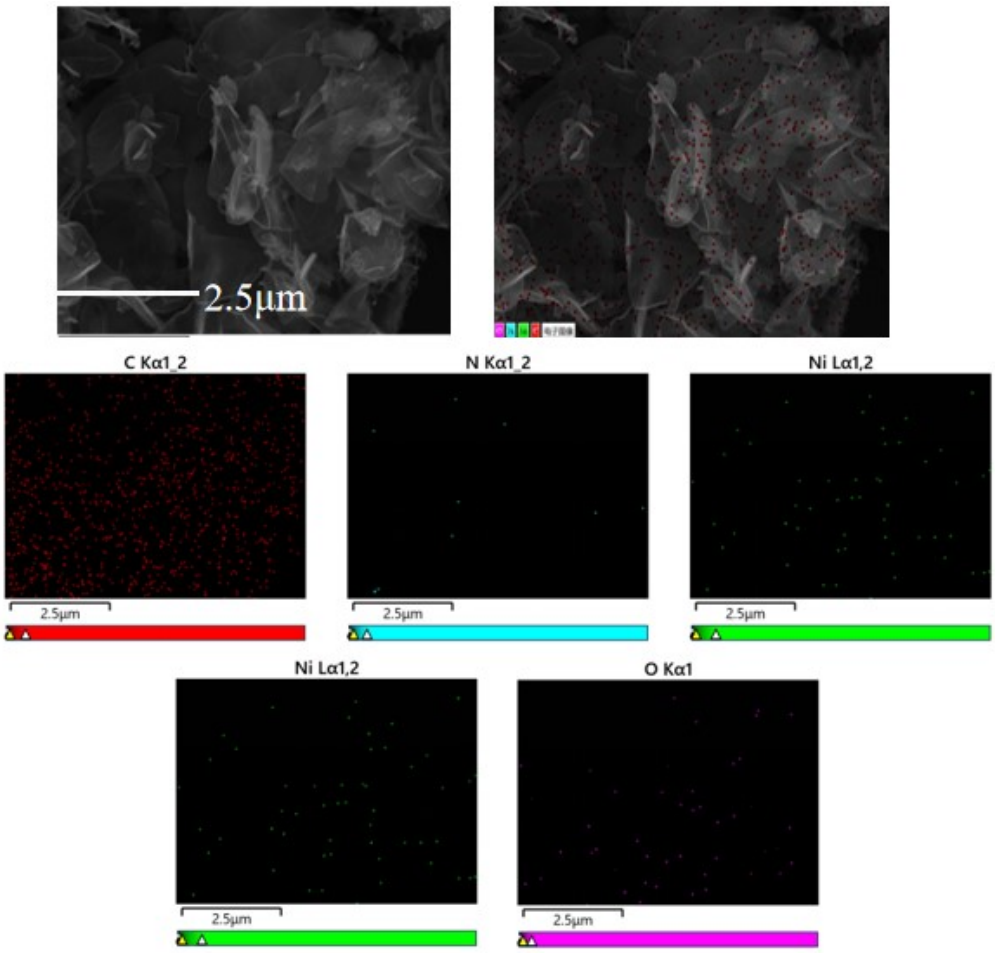

Figure S7. EDS of Ni-N-CNS.

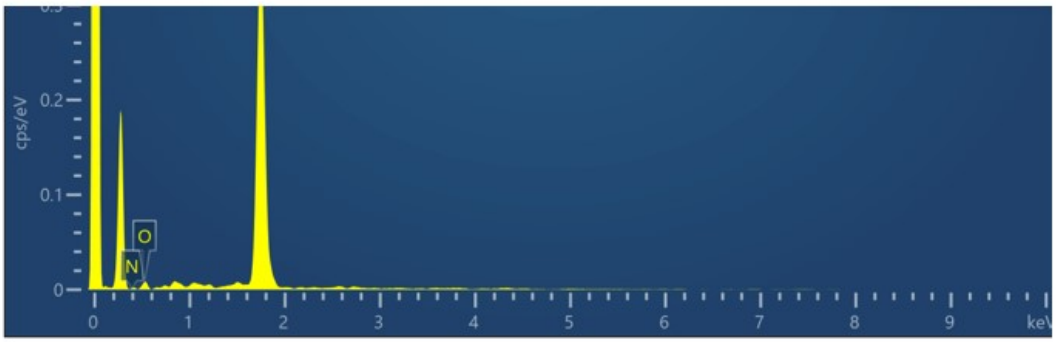

Element	Spectra type	Weight percentage	Wt % Sigma	Atomic percentage
C	K series spectra	82.87	5.71	88.99
N	K series spectra	3.64	5.37	3.36
O	K series spectra	7.99	2.21	6.44
Ni	L series spectra	5.49	3.05	1.21
Total content		100.00		100.00

XPS of Ni-N-CNS				
Name	Peak BE	FWHM eV	Area(P) CPS.eV	Atomic %
C1s	285.01	3.17	1159144.48	84.98
O1s	531.84	3.87	251579.38	7.26
N1s	399.39	4.31	148557.29	6.86
Ni2p	855.11	3.63	177175.83	0.9

Figure S8. Comparison of element content results between EDS and XPS of Ni-N-CNS.

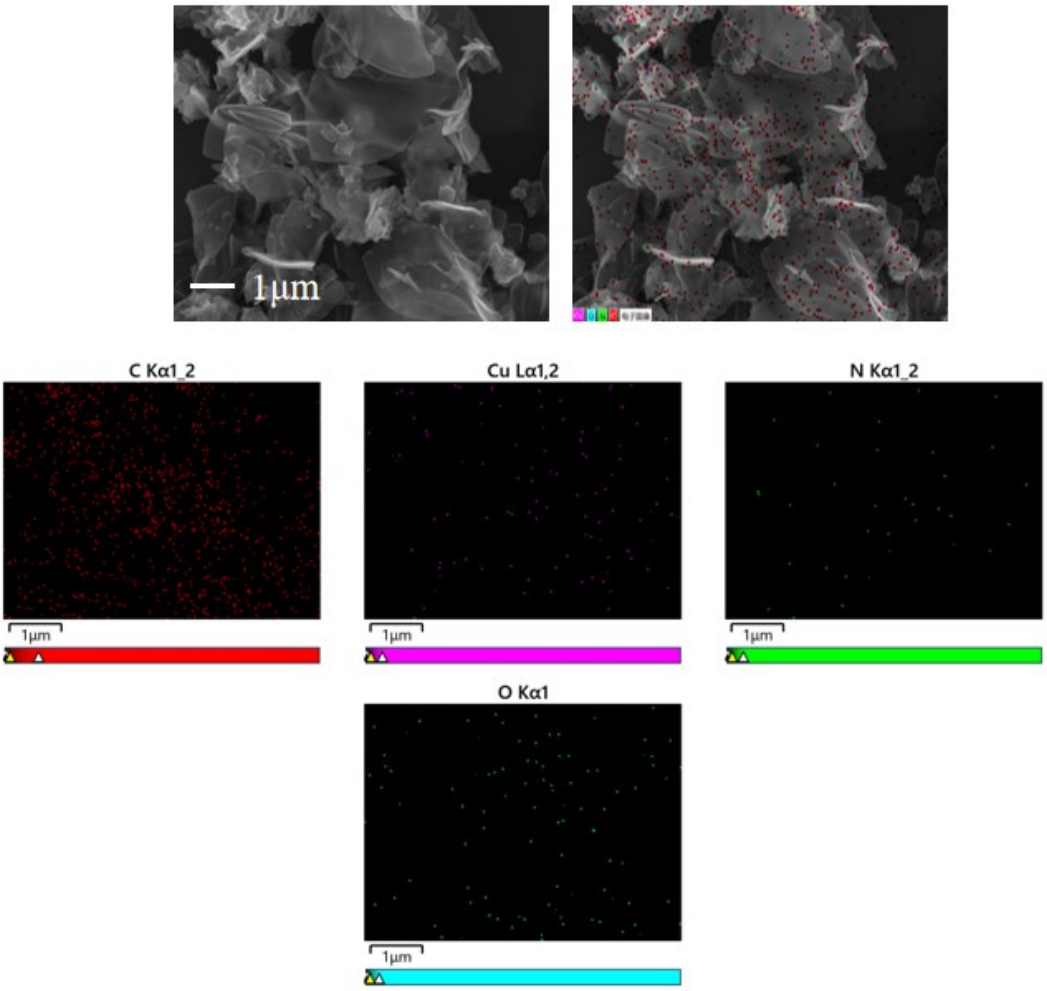

Figure S9. EDS of Cu-N-CNS.

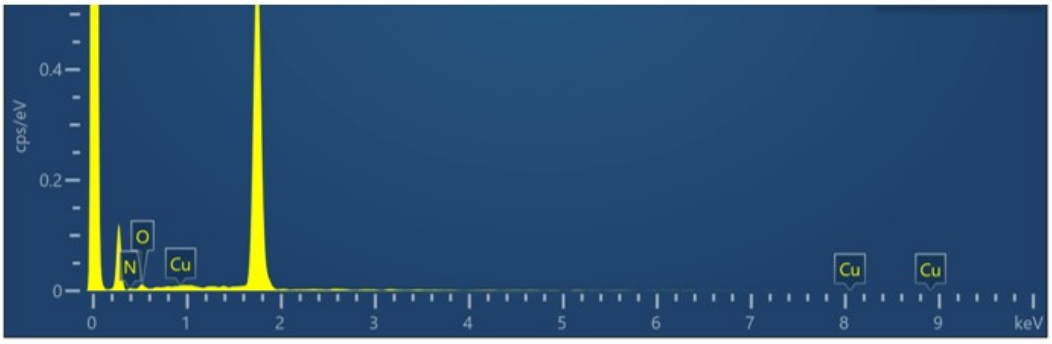

Element	Spectra type	Weight percentage	Wt % Sigma	Atomic percentage
C	K series spectra	76.47	7.93	80.65
N	K series spectra	10.61	7.92	9.60
O	K series spectra	12.12	3.63	9.60
Cu	L series spectra	0.80	3.55	0.16
Total content		100.00		100.00

XPS of Cu-N-CNS				
Name	Peak BE	FWHM eV	Area(P) CPS.eV	Atomic %
C1s	285.01	3.15	1067842.19	83.88
O1s	531.92	3.8	283323.24	8.77
N1s	399.27	4.4	85736.32	6.96
Cu2p	934.67	3.17	177175.83	0.39

Figure S10. Comparison of element content results between EDS and XPS of Cu-N-CNS.

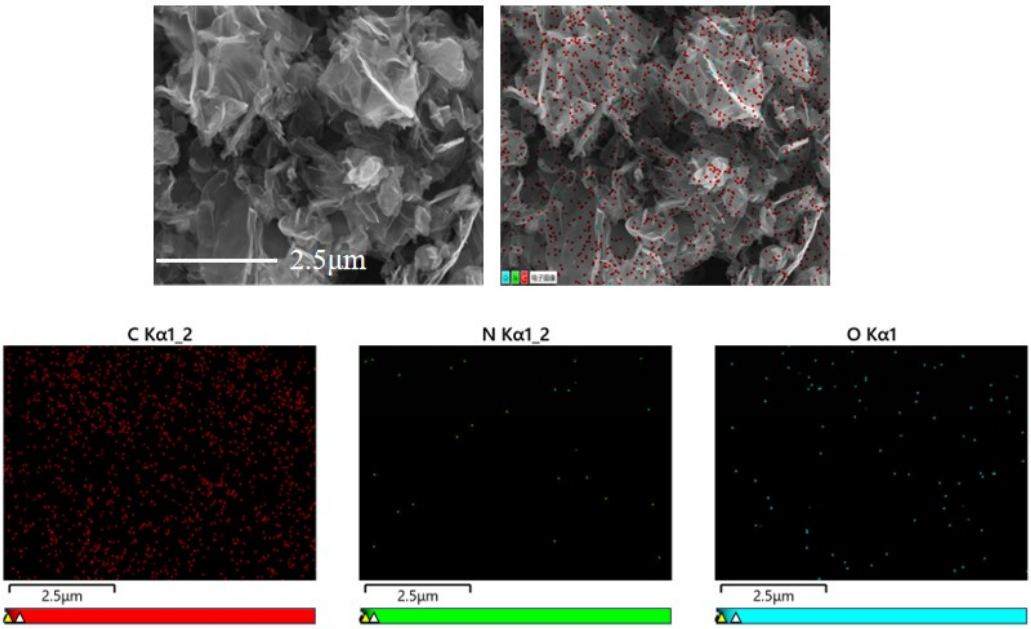

Figure S11. EDS of N-CNS.

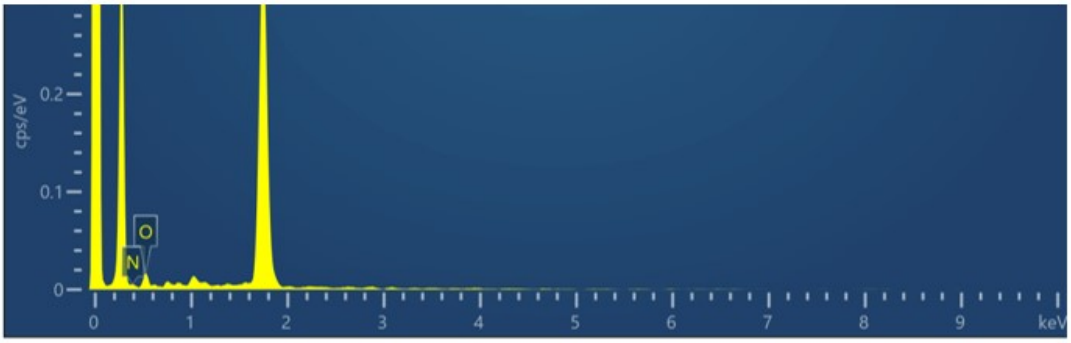

Element	Spectra type	Weight percentage	Wt % Sigma	Atomic percentage
C	K series spectra	82.63	5.12	85.63
N	K series spectra	7.77	5.29	6.91
O	K series spectra	9.60	2.13	7.47
Total content		100.00		100.00

XPS of N-CNS				
Name	Peak BE	FWHM eV	Area(P) CPS.eV	Atomic %
C1s	285.02	3.16	1033573.06	84.47
O1s	531.91	3.87	249591.97	8.03
N1s	399.35	4.49	145665.49	7.5

Figure S12. Comparison of element content results between EDS and XPS of N-CNS.

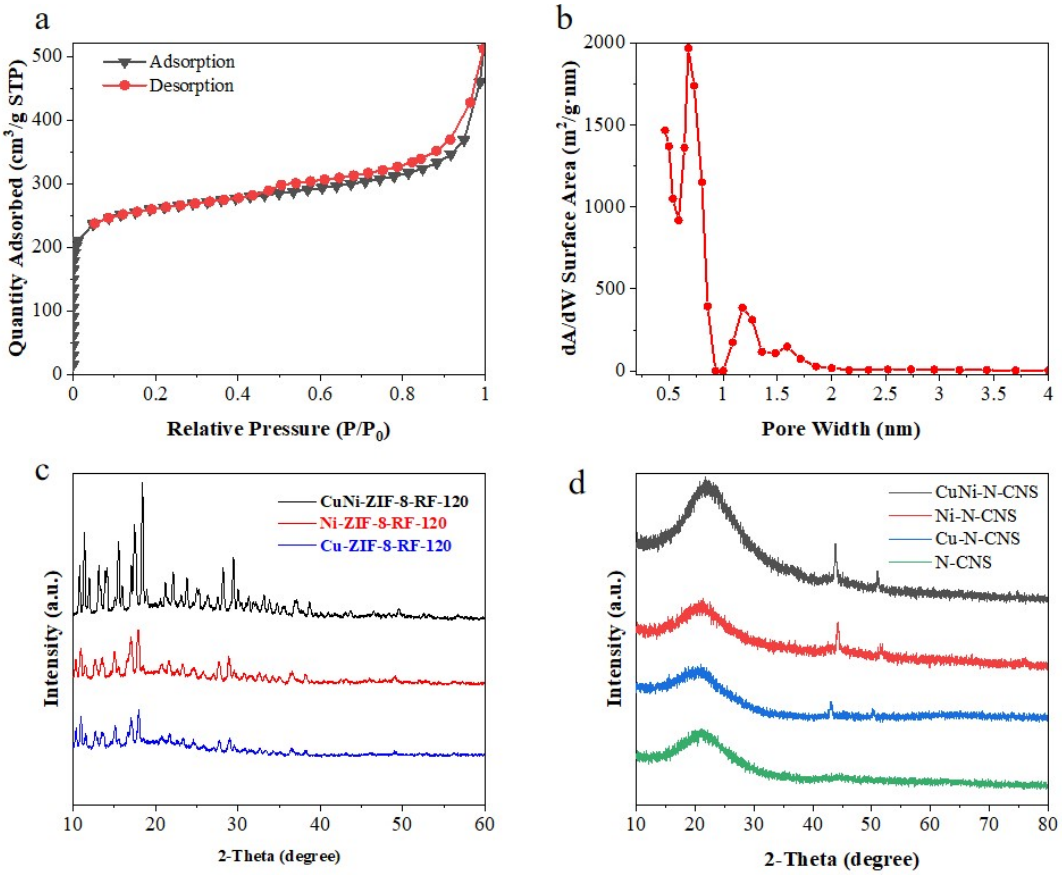

Figure S13. (a) N_2 sorption isotherms of CuNi-N-CNS. (b) Pore size distribution. (c) X-ray diffraction patterns of CuNi-ZIF-8-RF-120 ℃, Ni-ZIF-8-RF-120 ℃ and Cu-ZIF-8-RF-120 ℃. (d) X-ray diffraction patterns of CuNi-N-CNS, Ni-N-CNS, Cu-N-CNS and N-CNS.

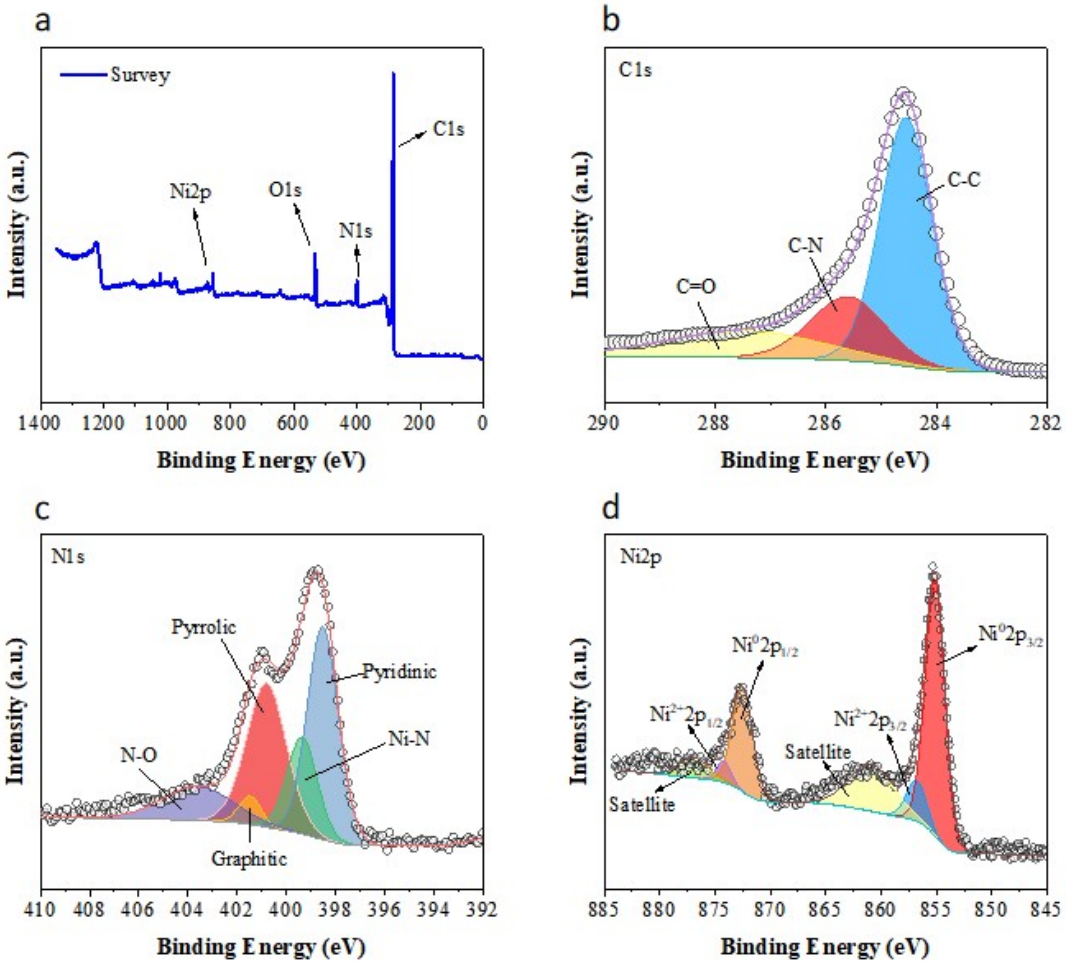

Figure S14. (a) The survey XPS spectrums of Ni-N-CNS. (b-d) High-resolution spectrums of C1s, N1s and Ni2p of Ni-N-CNS.

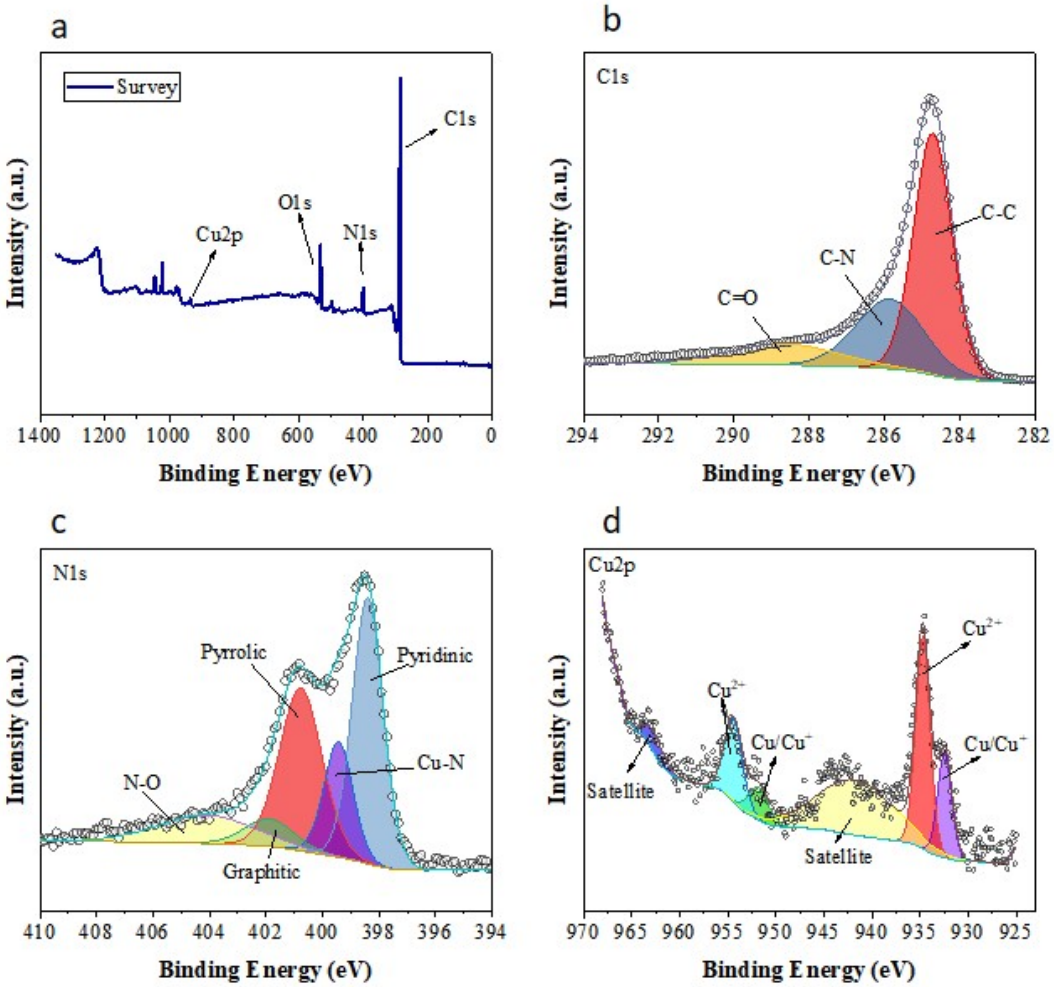

Figure S15. (a) The survey XPS spectrums of Cu-N-CNS. (b-d) High-resolution spectrums of C1s, N1s and Cu2p of Cu-N-CNS.

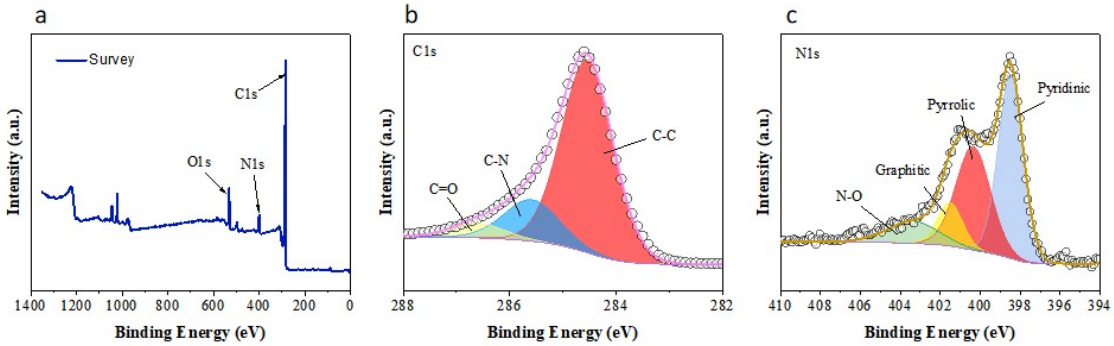

Figure S16. (a) The survey XPS spectrums of N-CNS. (b-c) High-resolution spectrums of C1s and N1s of N-CNS.

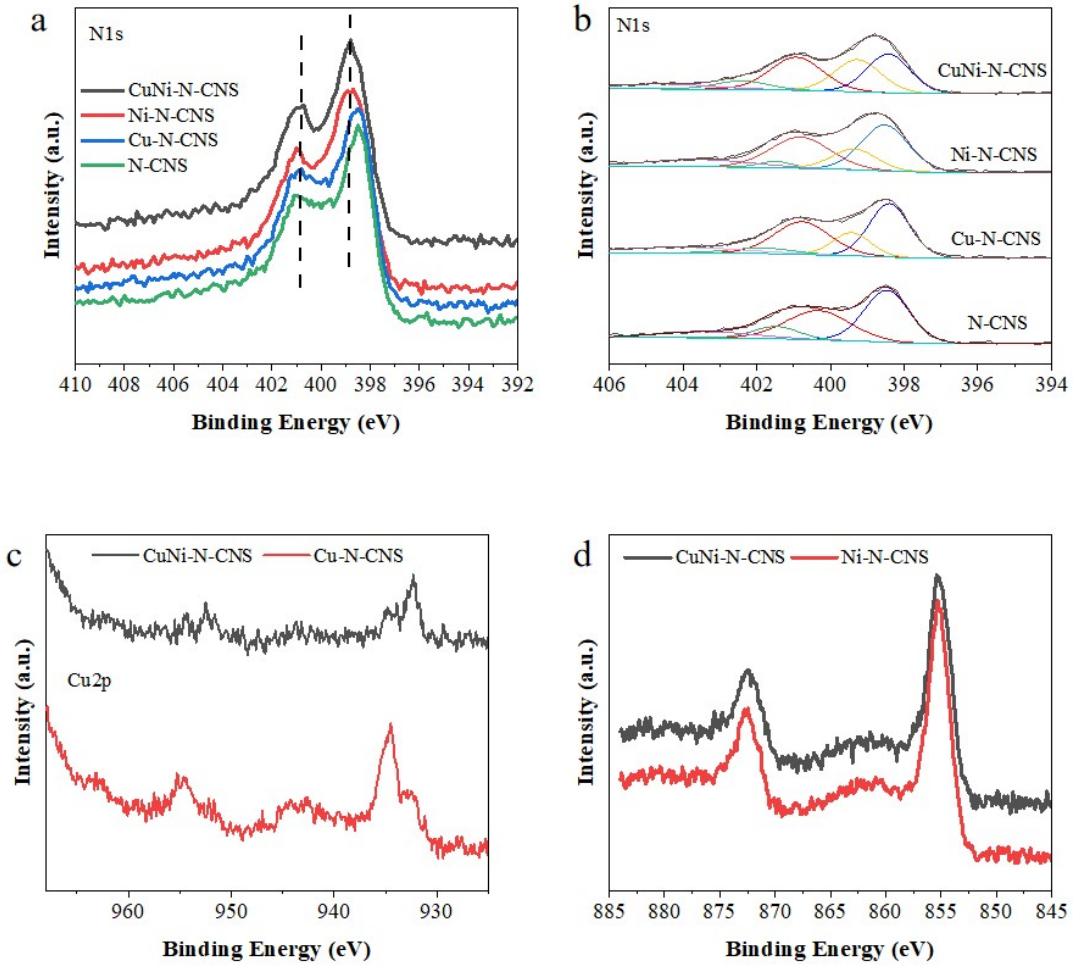

Figure S17. The energy shift in the spectrum of CuNi-N-CNS compared with controlled sample.

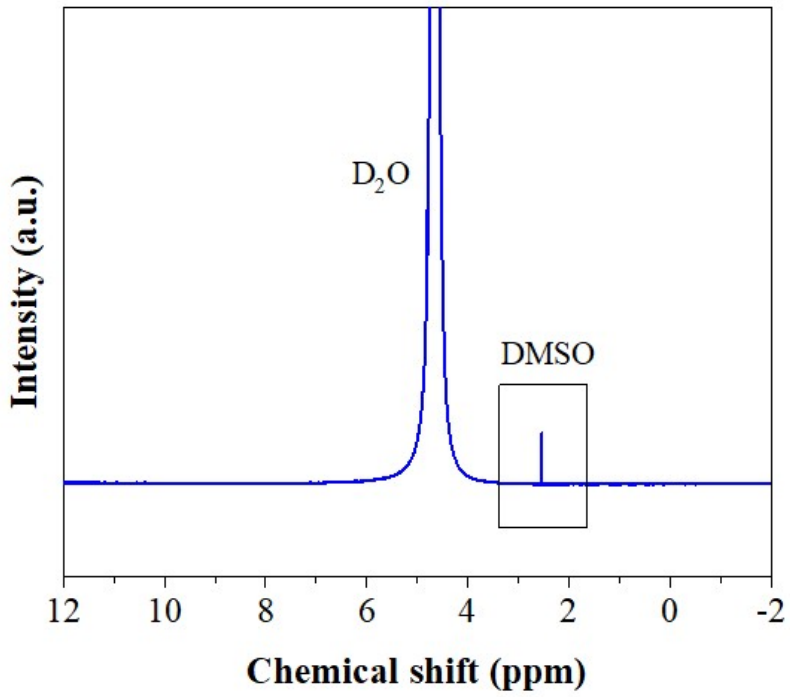

Figure S18. [1]HNMR result of liquid products after electrolysis. The result shows that no liquid product is generated.

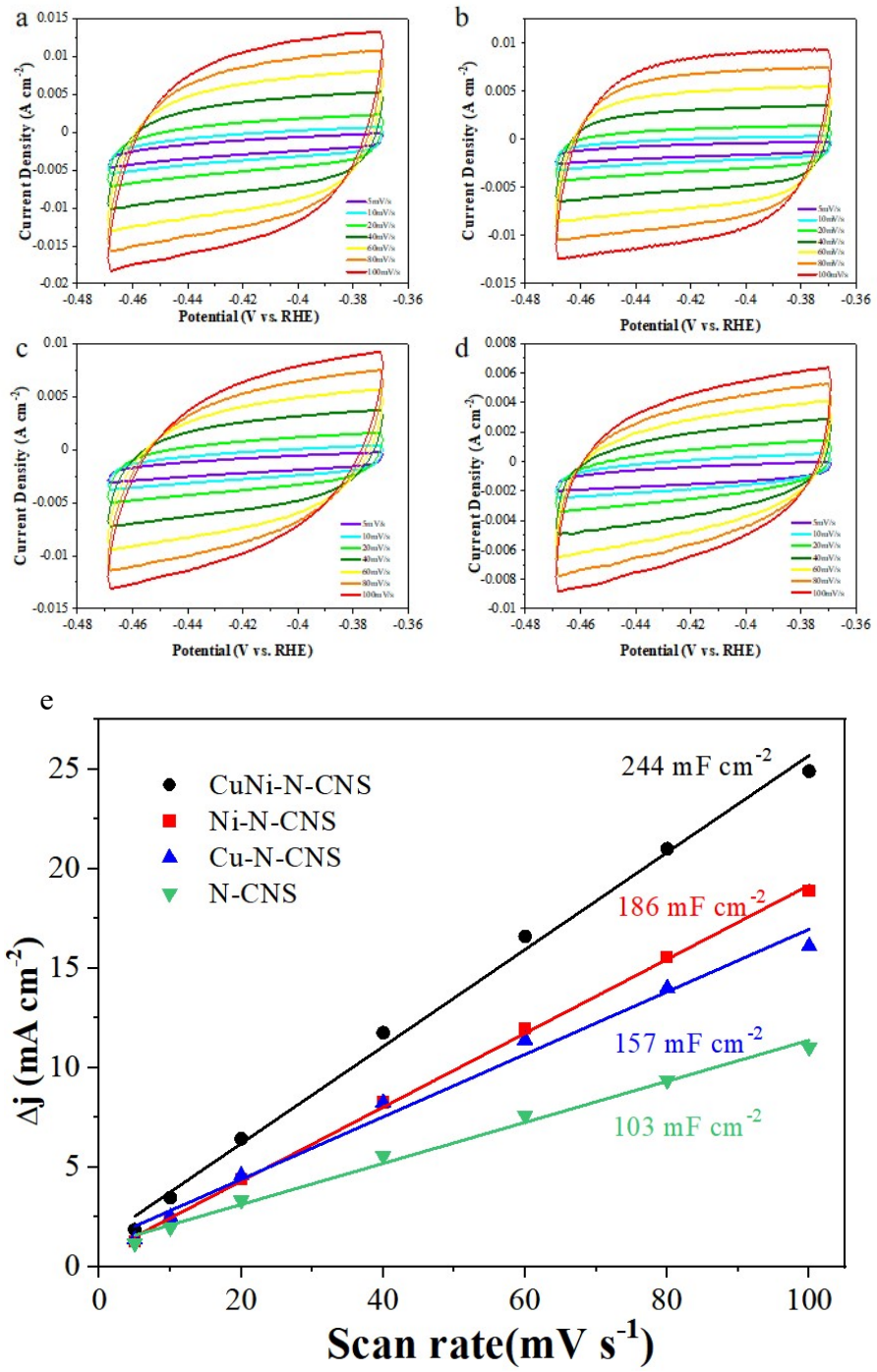

Figure S19. (a-d) CV curves of CuNi-N-CNS, Ni-N-CNS, Cu-N-CNS and N-CNS. (e) ECSAs of CuNi-N-CNS, Ni-N-CNS, Cu-N-CNS and N-C.

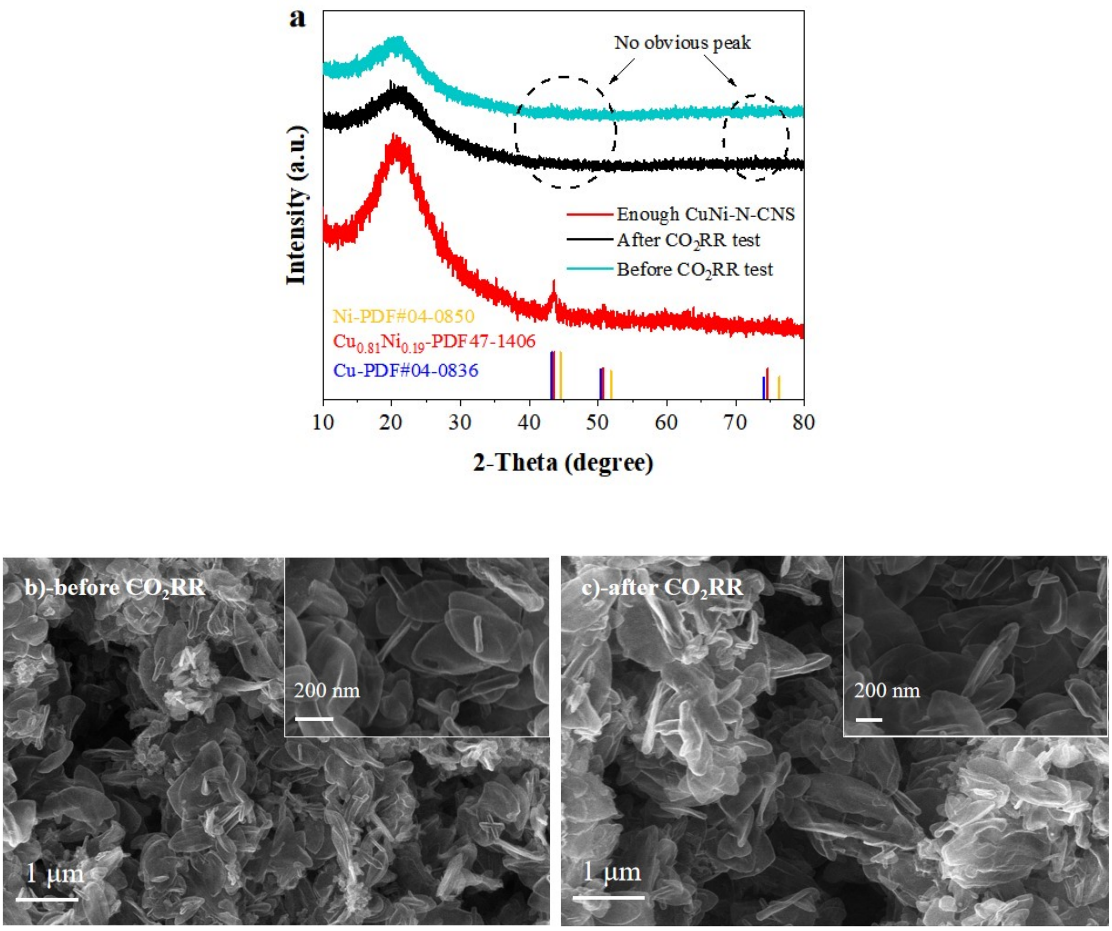

Figure S20. (a) XRD patterns of enough CuNi-N-CNS powder, small amount of samples scraped from carbon paper before and after electrolysis. (b-c) SEM images of CuNi-N-CNS before and after CO_2RR.

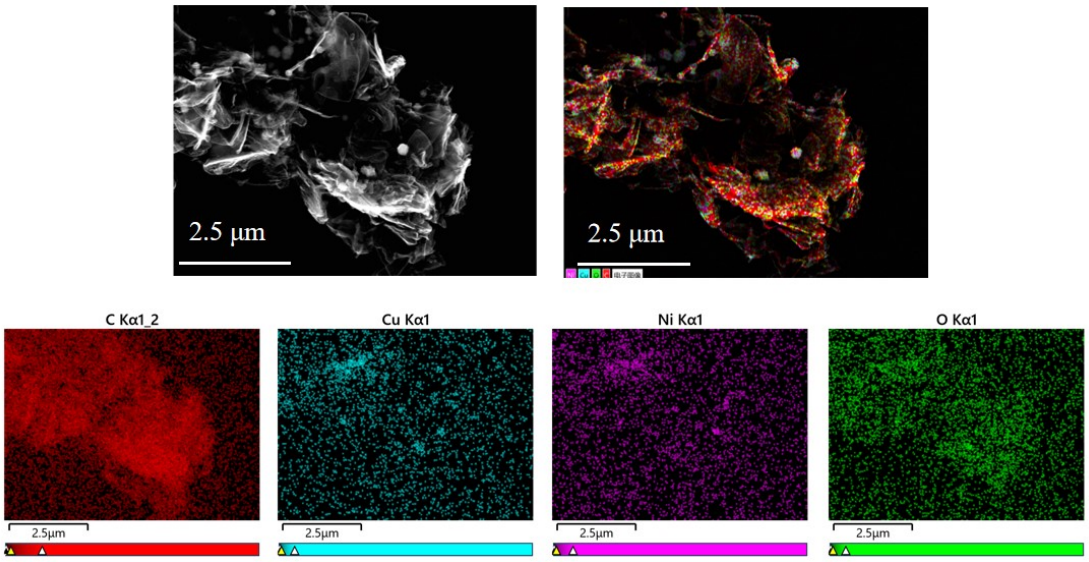

Figure S21. Element mapping of CuNi-N-CNS after electrolysis.

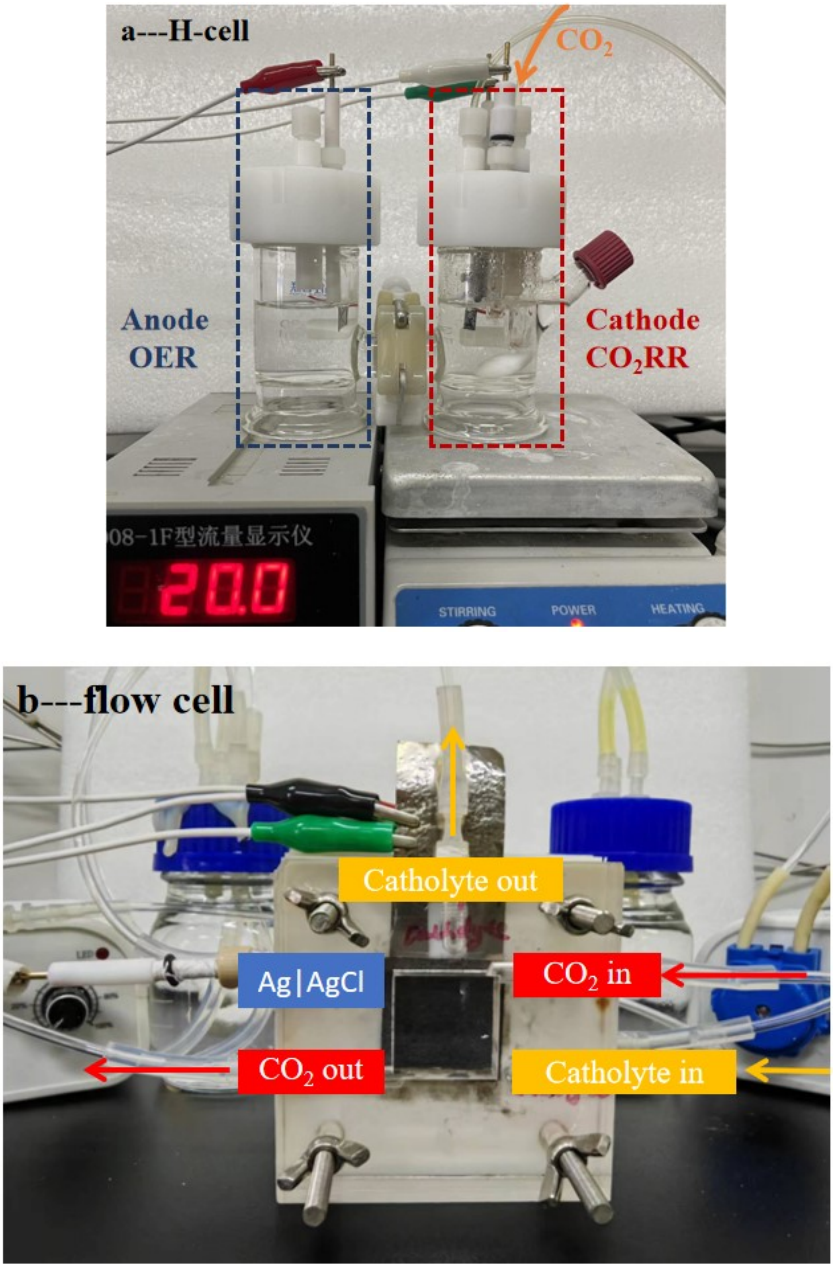

Figure S22. H-cell and self-assembly flow cell.

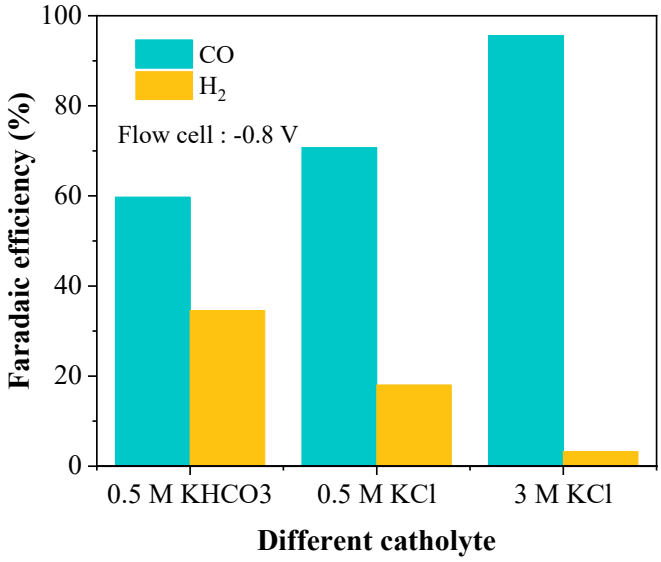

Figure S23. Effects of different electrolytes and concentrations on product distribution at -0.8 V.

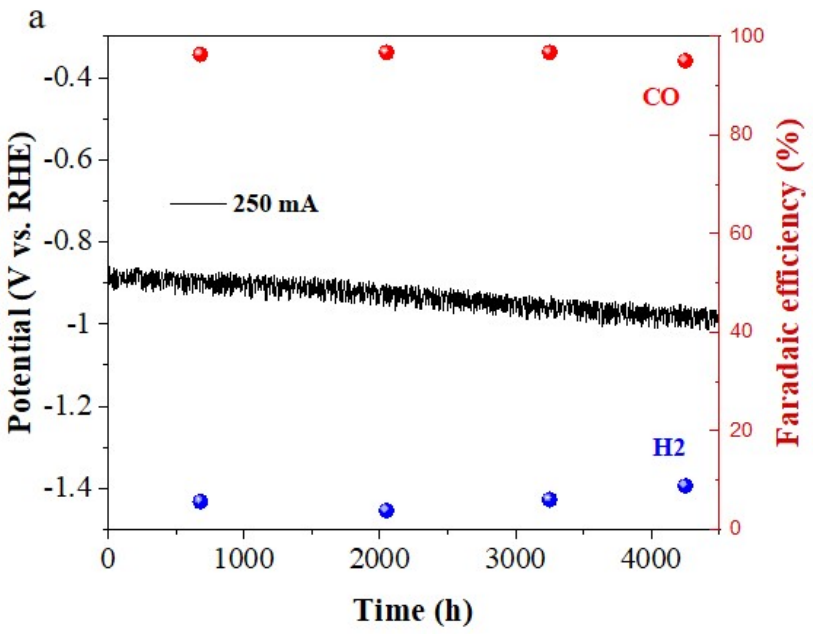

Figure S24. Potential-time response of CuNi-N-CNS in three-electrode flow cell for CO_2RR and the corresponding faradaic efficiency for CO/H_2 production at current densities of 250 mA cm^{-2}.

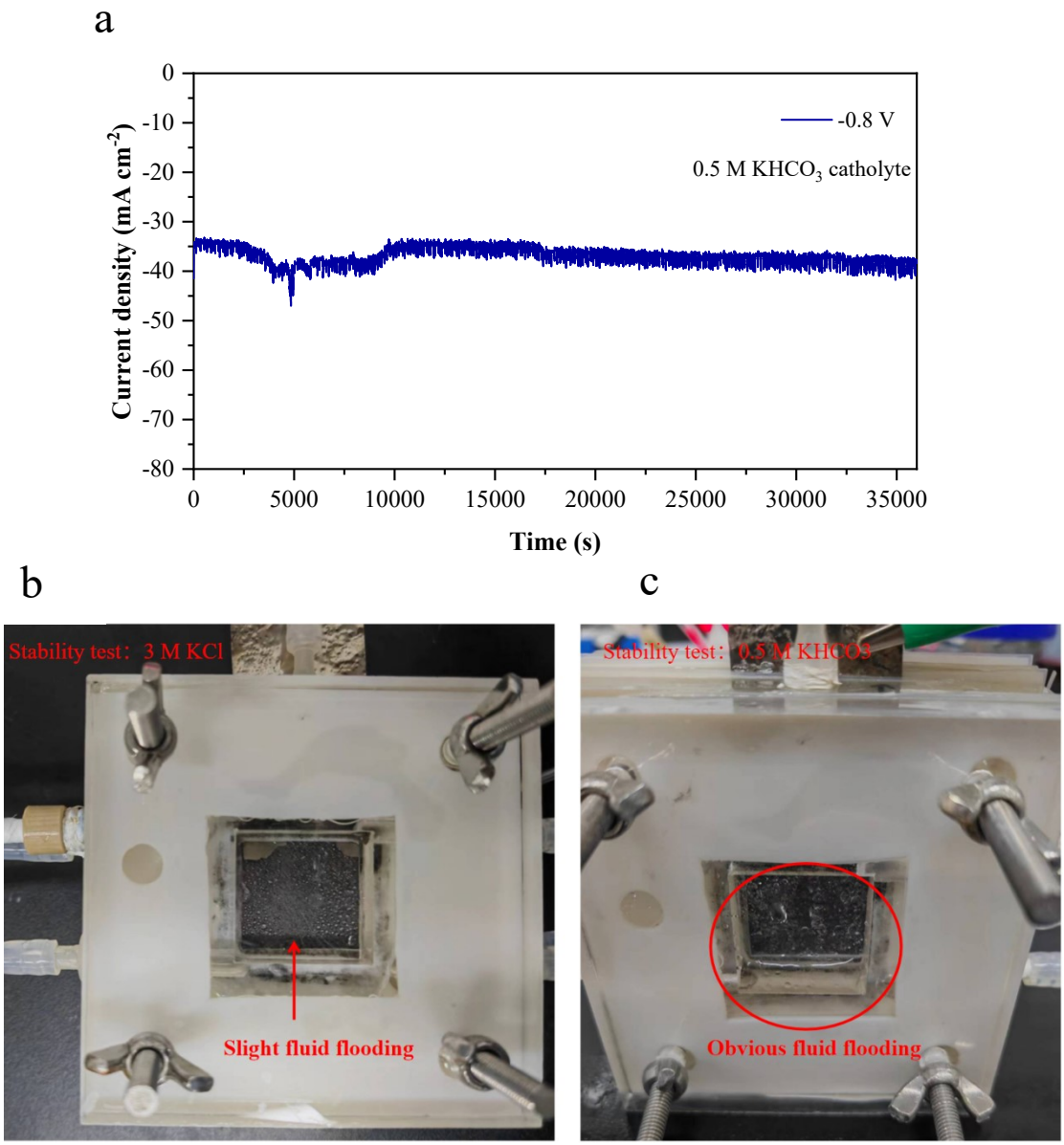

Figure S25. (a) Long-term test of CuNi-N-CNS in flow cell with 0.5 M $KHCO_3$ solution as catholyte. (b-c) Comparison of liquid flooding after stability test with different catholytes.

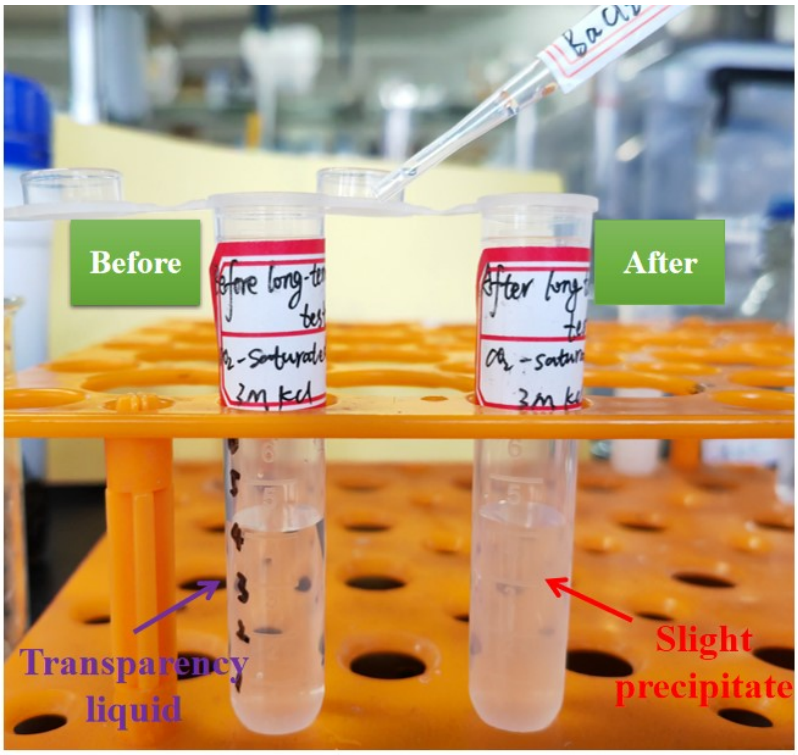

Figure S26. Precipitation experiment.

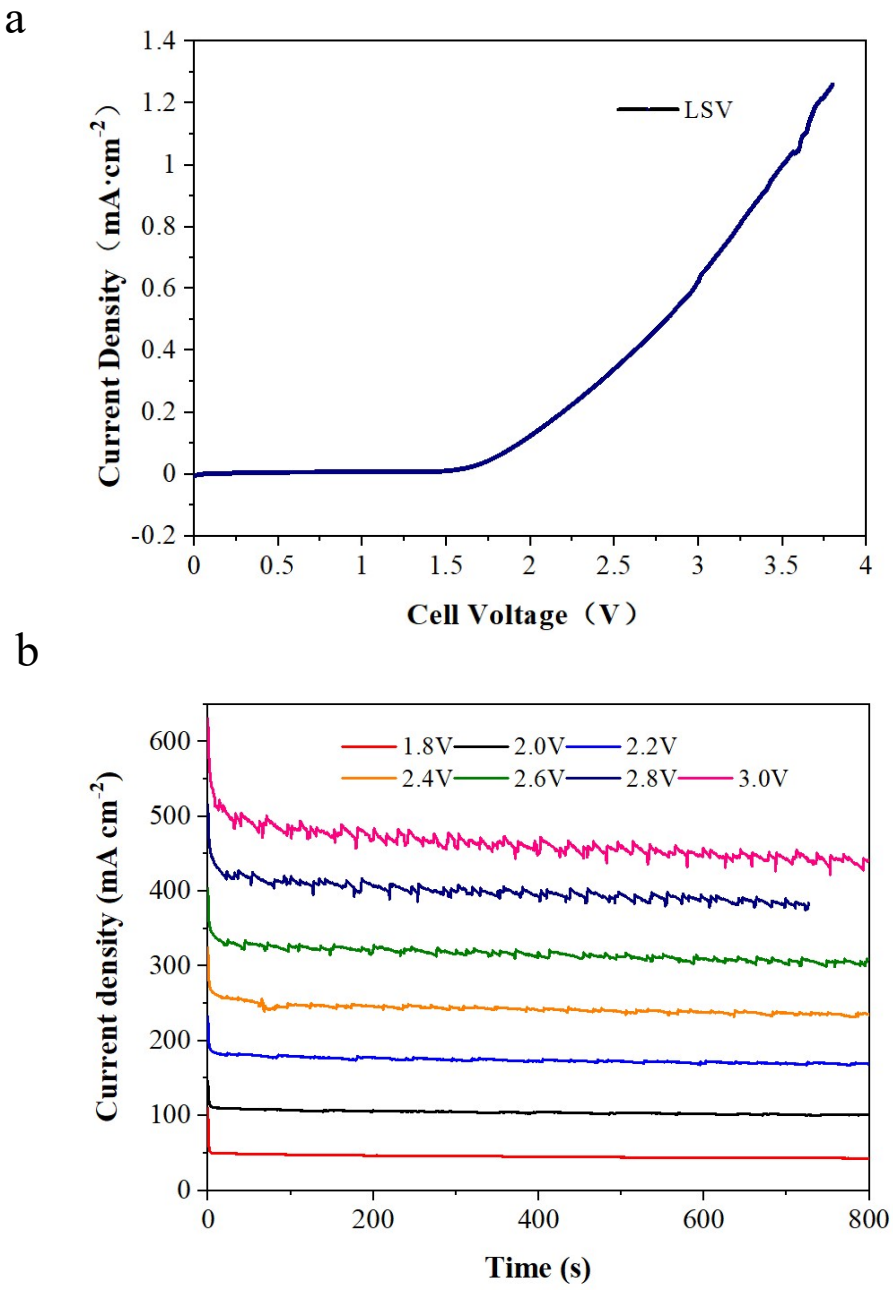

Figure S27. (a) LSV and (b) i-t curves of two-electrode system in flow cell.

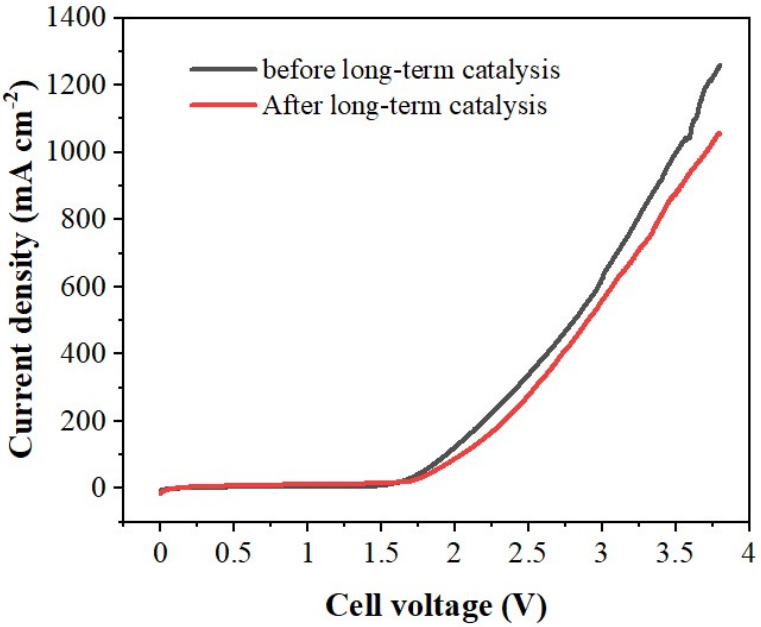

Figure S28. LSV curves comparison before and after long-term stability test. The performance was not degraded much after long-term stability test.

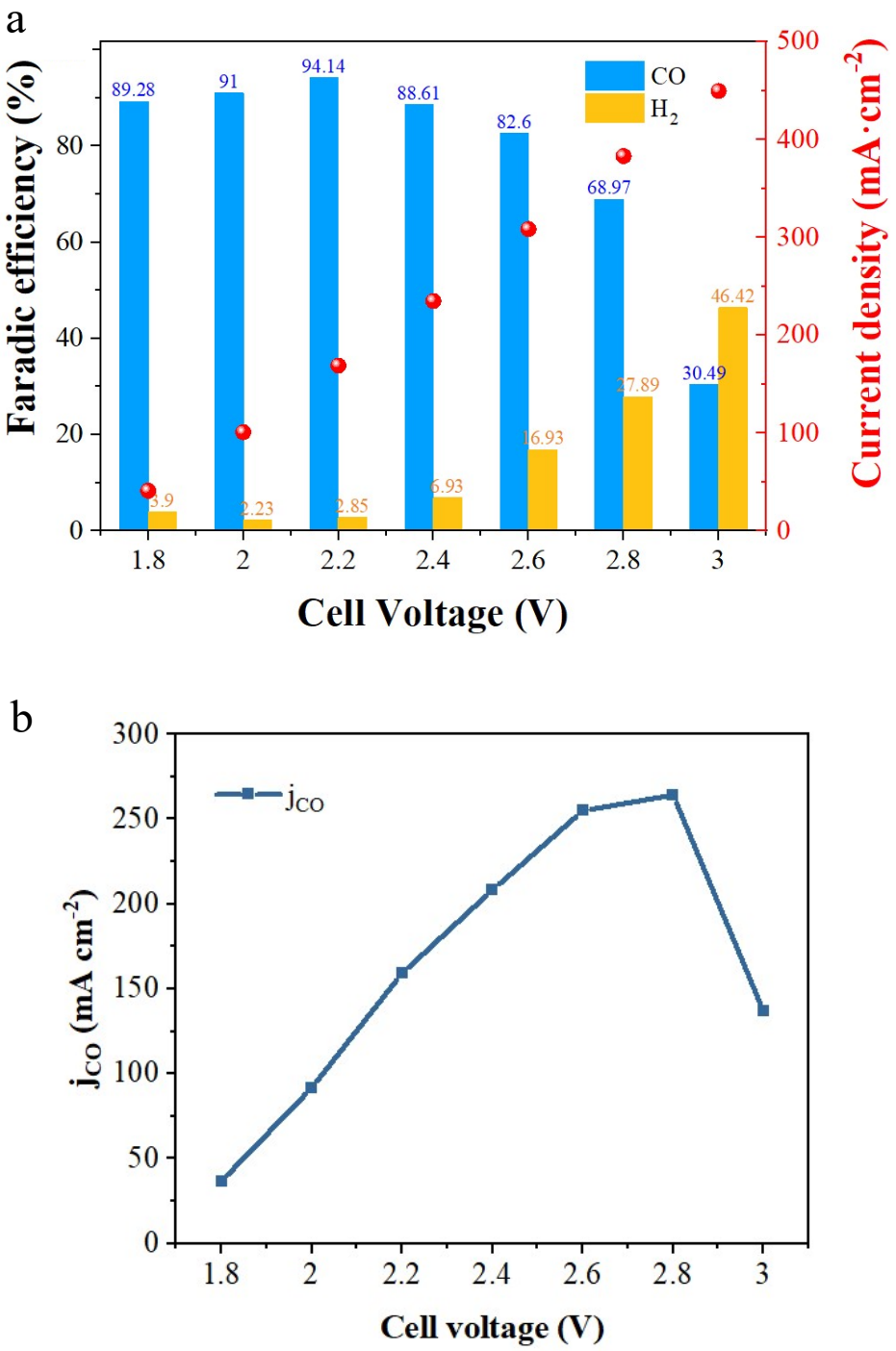

Figure S29. (a) FE_{CO} and (b) j_{CO} of different potentials.

Reference

1 H. Cheng, X. Wu, M. Feng, X. Li, G. Lei, Z. Fan, D. Pan, F. Cui and G. He, Atomically Dispersed Ni/Cu Dual Sites for Boosting the CO_2 Reduction Reaction, *ACS Catal.*, 2021, **11**, 12673-12681.

2 Z. Chen, X. Zhang, W. Liu, M. Jiao, K. Mou, X. Zhang and L. Liu, Amination strategy to boost the CO_2 electroreduction current density of M–N/C single-atom catalysts to the industrial application level, *Energy Environ. Sci.*, 2021, **14**, 2349-2356.

3 Y. Cheng, S. Zhao, H. Li, S. He, J.-P. Veder, B. Johannessen, J. Xiao, S. Lu, J. Pan, M. F. Chisholm, S.-Z. Yang, C. Liu, J. G. Chen and S. P. Jiang, Unsaturated edge-anchored Ni single atoms on porous microwave exfoliated graphene oxide for electrochemical CO_2, *Appl. Catal. B Environ.*, 2019, **243**, 294-303.

4 Y. Gang, E. Sarnello, J. Pellessier, S. Fang, M. Suarez, F. Pan, Z. Du, P. Zhang, L. Fang, Y. Liu, T. Li, H.-C. Zhou, Y. H. Hu and Y. Li, One-Step Chemical Vapor Deposition Synthesis of Hierarchical Ni and N Co-Doped Carbon Nanosheet/Nanotube Hybrids for Efficient Electrochemical CO_2 Reduction at Commercially Viable Current Densities, *ACS Catal.*, 2021, **11**, 10333-10344.

5 K. Jiang, S. Siahrostami, T. Zheng, Y. Hu, S. Hwang, E. Stavitski, Y. Peng, J. Dynes, M. Gangisetty, D. Su, K. Attenkofer and H. Wang, Isolated Ni single atoms in graphene nanosheets for high-performance CO_2 reduction, *Energy Environ. Sci.*, 2018, **11**, 893-903.

6 W. Ren, X. Tan, W. Yang, C. Jia, S. Xu, K. Wang, S. C. Smith and C. Zhao, Isolated Diatomic Ni-Fe Metal-Nitrogen Sites for Synergistic Electroreduction of CO_2, *Angew. Chem., Int. Ed.*, 2019, **58**, 6972-6976.

7 W. Xiong, H. Li, H. Wang, J. Yi, H. You, S. Zhang, Y. Hou, M. Cao, T. Zhang and R. Cao, Hollow Mesoporous Carbon Sphere Loaded Ni-N4 Single-Atom: Support Structure Study for CO_2 Electrocatalytic Reduction Catalyst, *Small*, 2020, **16**, e2003943.

8 H. Yang, Q. Lin, C. Zhang, X. Yu, Z. Cheng, G. Li, Q. Hu, X. Ren, Q. Zhang, J. Liu and C. He, Carbon dioxide electroreduction on single-atom nickel decorated carbon membranes with industry compatible current densities, *Nat. Commun.*, 2020, **11**, 593.